Broadband acoustic metalaser for continuous sine waves and pulses

Xudong Fan,[1,2,*] Qi Jin,[1] Haicai Xiao,[1] Yang Kang,[1] Xiaolong Huang,[1] Can Li,[1] Ning Li,[1] and Chunsheng Weng[1]

[1] *National Key Laboratory of Transient Physics, Nanjing University of Science and Technology, Nanjing, 210094, China*

[2] *Ministry of Education Key Laboratory of Modern Acoustics, Nanjing University, Nanjing, 210093, China*

(Received 11 September 2023; revised 6 November 2023; accepted 5 December 2023; published 14 December 2023)

We propose a broadband acoustic metalaser that can effectively concentrate incident acoustic energy on the central axis for a long distance. The acoustic metalaser is axisymmetric and consists of a series of concentric-ring-like structures. By adjustment of the geometric parameters of the structure, the transmitted phase can be effectively controlled, and an energy-concentrated beam with a central pressure maximum along the beam axis can be generated. Because of the similar phase tendency of the metastructure at different frequencies, the same structure could achieve broadband acoustic energy convergence without the need for changes. We examine the broadband performance of the proposed metalaser using continuous sine waves of different frequencies from 2.5 to 18 kHz numerically and experimentally. In addition, the propagation of pulse waves with relative bandwidths of 53% and 117% through the metalaser is also investigated in the transient domain, where the effect of the acoustic metalaser on a broadband signal containing multiple frequencies is examined simultaneously. The results prove the ability of the metalaser for broadband acoustic energy convergence while the signal envelope is kept almost unchanged. Our work should find applications in many fields where the convergence of broadband or pulsed acoustic signals is desired.

DOI: 10.1103/PhysRevApplied.20.064026

I. INTRODUCTION

The convergence of acoustic energy is an important phenomenon and also plays a significant role in many fields, such as acoustic imaging [1] and particle manipulations [2,3]. Unlike conventional natural acoustic materials with a large size and a curved shape or active speaker arrays with complex signal-processing systems and high cost, recently emerged acoustic metamaterials and metasurfaces [4–7] exhibit ability for the convergence of acoustic energy by directly tailoring the transmitted and/or reflected phase delay. There are several types of metamaterial that are commonly used for the precise manipulation of acoustic waves; for example, labyrinthine metamaterials of either reflected type [8] or transmitted type (single layer [9,10], double layers [11] and a helical structure [12]), Helmholtz resonators [13–16], metagratings [17, 18], coding metamaterials [19,20], and lossy metamaterials [21,22]. Fascinating focusing phenomena have been achieved by acoustic metamaterials with the advantages of planar configuration, subwavelength thickness, low cost, and high efficiency [23–25]; however, previous reflection-type metamaterials suffer from the aliasing of the incident and reflected fields and most of the transmissive designs have limited working bandwidths due to specific resonance mechanisms. These drawbacks tremendously limit practical applications such as nondestructive evaluation and acoustic imaging. With regard to this, the study of broadband transmissive-type metamaterials to effectively extend the working frequency bandwidth and simplify the applications has attracted much attention [26–28]. Extraordinary success has broadened the potential applications for acoustic focuses; however, in most previous studies, the behaviors of metamaterials or metasurfaces were studied only in the frequency domain, where the behaviors of metamaterials and metasurfaces for different frequencies were dealt with individually (i.e., monochromatic sine waves), and the investigation of real broadband time-domain signals containing multiple frequencies simultaneously is missing.

In this work, we propose an acoustic metalaser for the broadband convergence of acoustic energy on the central axis for a long range. The metalaser is axisymmetric and is composed of a series of concentric-ring-like structures. By adjustment of the abrupt cross section of the concentric-ring-like structure, the transmitted phase can be effectively controlled and modulated to cover the entire 2π range. The propagation of continuous sine waves of different frequencies through the metalaser is first investigated numerically

*fanxudong@njust.edu.cn

and experimentally in the frequency domain. Then, broadband pulse waves with relative bandwidths of 53% and 117% are directly used to examine the performance of the acoustic metalaser in the transient domain, where the effect on broadband incident waves containing multiple frequencies is investigated and studied simultaneously. The results prove the ability and effectiveness of the acoustic metalaser proposed here for the broadband convergence of acoustic energy while the signal envelope is kept almost unchanged. Our work should help the further investigation of acoustic energy concentration and harvesting, which is applicable in many fields, such as acoustic imaging, ultrasound therapy, and particle manipulation, and other broadband devices.

II. DESIGN OF THE CONCENTRIC-RING-LIKE METALASER

The acoustic metalaser for the convergence of acoustic energy proposed here is illustrated in Fig. 1(a), where the metalaser consists of a series of ringlike structures with the same width W. Figure 1(b) shows an enlargement of part of the ringlike structure shown in Fig. 1(a), where the height h, the width W, and the wall thickness t of the structure are 5 cm, $0.2h$ and $0.05W$, respectively. The structure consists of several straight panels, which create a series of abrupt cross sections within the straight channel. Hence, by adjustment of the ratio of the sharp change of the cross section, i.e., w/W, the transmitted phase of the pressure field can be effectively controlled to cover the full 2π range, with the simulated results shown in Fig. 1(c). Eight discrete phases used for the construction of the acoustic metalaser are indicated by the eight black circles. The inset in Fig. 1(c) shows the transmitted phases when the frequency f and the geometric parameter w/W are varied. From the results, the phase response of the same structure varies with the working frequency; the phase-response tendency, however, is similar within a broad frequency bandwidth, indicating that the same metalaser could be potentially used for broadband manipulations of the incident acoustic waves with no need for any changes of the structure.

The transmitted-phase profile, $\Phi(r)$, on the interface of the metalaser satisfies the generalized Snell's law of refraction with the following form for normally incident plane waves [29]: $k\sin\theta_t = d\Phi(r)/dr$, where $k = 2\pi/\lambda$ is the wave number, with λ being the wavelength, θ_t is the refraction angle, and r is the transverse coordinate in the cylindrical coordinate system.

For the convergence of acoustic energy considered here, the phase distribution on the surface of the metalaser is axisymmetric around the z axis and independent of the azimuthal angle ϕ. To concentrate acoustic energy on the central z axis for a long propagation distance, an acoustic Bessel beam with paraxial parameter $\beta = 15^\circ$ is generated as an example, with the phase profile along the r direction being [29]

$$\Phi(r) = kr\sin\beta = kr\sin 15^\circ. \tag{1}$$

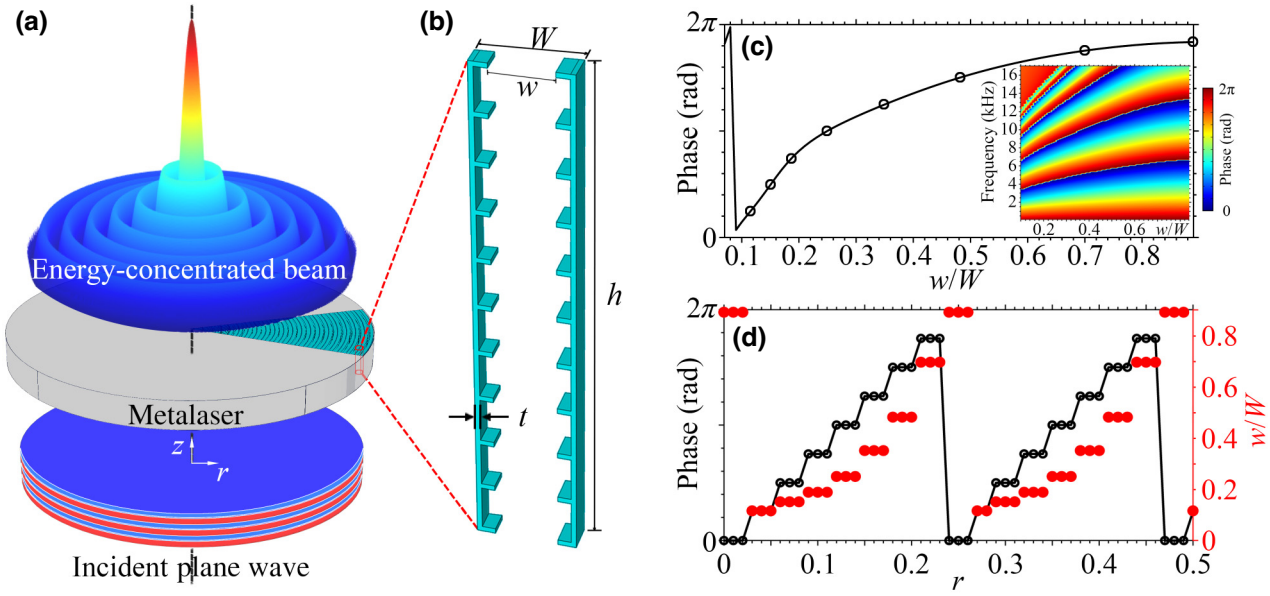

FIG. 1. (a) Concentration of acoustic energy via an acoustic metalaser, which is axisymmetric and composed of a series of concentric-ring-like structures. (b) Part of the concentric-ring-like structure of the metalaser. (c) Transmitted phase of the pressure field at a frequency of 5700 Hz. The eight black circles correspond to eight discrete phases covering the 2π range. The inset shows transmitted phases when the frequency f and the geometric parameter w/W are varied. (d) Profiles of the transmitted phase and the geometric parameter along the r direction.

The phase profile for the metalaser is shown in Fig. 1(d), and the corresponding distribution of the geometric parameter w/W is, in turn, obtained with the aid of the results in Fig. 1(c) at 5700 Hz. Note that the angle of 15° chosen here is not mandatory, but generally speaking, the propagation range of the acoustic laser will increase as the angle decreases.

III. CONVERGENCE OF ACOUSTIC ENERGY FOR CONTINUOUS SINE WAVES

To examine the performance of the acoustic metalaser for the broadband convergence of acoustic energy, we first numerically simulate continuous sine plane waves transmitted through the same metalaser at different frequencies as illustrated in Fig. 1(a). The transmitted intensity fields for three typical frequencies, i.e., 4000, 8000, and 12 000 Hz, from the simulations are shown in Fig. 2(a). From the results, the acoustic metalaser here can effectively concentrate the incident acoustic energy on the central axis of the transmitted beam for a long distance, and the energy outside the beam center is much weaker, as expected. Corresponding transmitted fields within the regions marked by white boxes are measured, with a photograph of a sample of the metalaser being shown in Fig. 2(b). The experimental results further validate the extraordinary performance and broadband features of the metalaser proposed here. We examine the normalized intensity distribution (i.e., amplification, obtained by the transmitted intensity divided by the incident intensity) along the transverse r direction and axial z direction for the three frequencies considered here, with the results being shown in Figs. 2(c) and 2(d), respectively. From the results, acoustic energy is concentrated at the beam center for a long distance. We further examine the amplification for different frequencies from 2.5 to 18 kHz, with the results being shown in Fig. 3, where the maximum amplification is larger than 20 within the entire frequency range considered here. The results confirm the excellent performance of the acoustic metalaser proposed here for the broadband convergence of acoustic energy with no need for any change of the structure.

Here the simulations are conducted with COMSOL MULTIPHYSICS, which is commercial software based on the finite-element method. The interface of "Acoustic-Thermoviscous Acoustic Interaction, Frequency Domain" is used together with a 2D axisymmetric model. Perfectly matched layers are used for the outer boundaries of the computation domain to avoid reflection. A free triangular mesh with a maximum size of $\lambda/5$ is used within the main

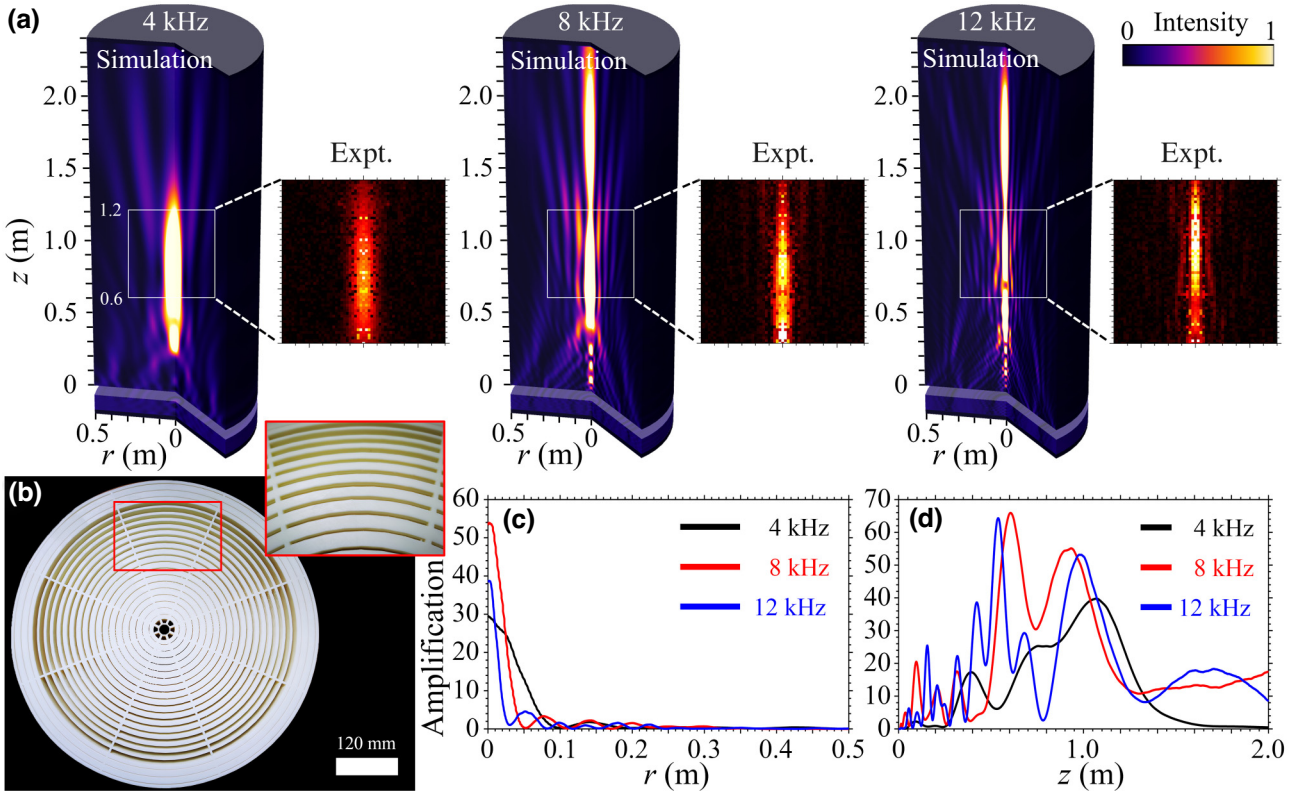

FIG. 2. (a) Measured and simulated transmitted intensity fields for continuous sine waves at different frequencies. (b) Photograph of a sample of the metalaser. (c) Transverse profile of the intensity amplification along the r direction at $z = 1$ m. (d) Axial profile of the intensity amplification along the z direction at $r = 0$.

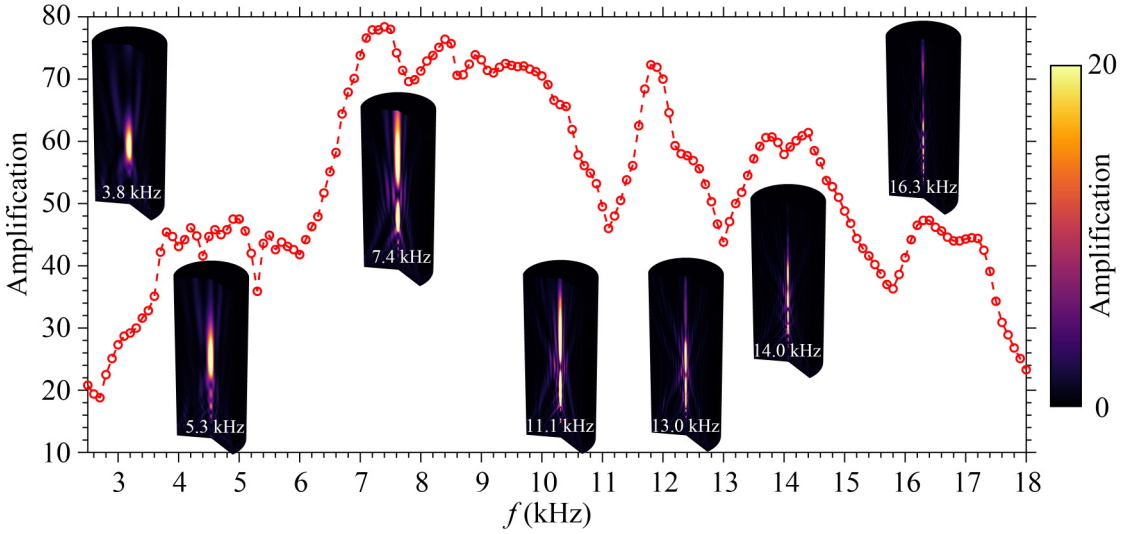

FIG. 3. Maximum values of the amplification for different frequencies. The insets show simulated acoustic intensity fields for 3.8, 5.3, 7.4, 11.1, 13.0, 14.0, and 16.3 kHz.

computation domain, and a mapped mesh of eight layers is used for the perfectly matched layers. Particularly, a finer mesh is configured near boundary layers to obtain acoustic fields precisely. The speed of sound and the mass density for the metalaser are 2278 m s^{-1} and 1100 kg m^{-3}, respectively, and for the background fluid they are 343 m s^{-1} and 1.21 kg m^{-3}, respectively. A parametric sweep of the incident frequency is used to examine the performance of the metalaser for different frequencies.

Besides, the sample of the metalaser shown in Fig. 2(b) was fabricated by 3D-printing technology with white epoxy resin. The sample is 60 cm in diameter and 5 cm in height. Transmitted acoustic fields were measured in a 2D cross section in free space. A loudspeaker with a diameter of 10 cm was fixed at the incident side of the metalaser. The speaker was connected to a signal generator and a power amplifier to generate steady sound signals for different frequencies, and a 1/4-in. microphone was used to measure transmitted acoustic intensity fields with a scanning resolution of 1 cm.

IV. CONVERGENCE OF ACOUSTIC ENERGY FOR BROADBAND PULSE WAVES

The acoustic metalaser here exhibits excellent ability for broadband convergence of acoustic energy. However, the previous simulations were conducted in the frequency domain, which means monochromatic incident plane waves (continuous sine waves of a single frequency) were used as the source. To directly examine the response and the performance of the acoustic metalaser for broadband incident waves with a certain bandwidth, we further simulate a broadband Gaussian wave packet transmitted through the metalaser. The Gaussian wave packet as a function of time t has the following form:

$$p = p_0 \exp\left[-\frac{(t-\mu)^2}{2\sigma^2}\right]\sin(2\pi f_0 t), \tag{2}$$

where p_0 is a constant pressure, μ and σ are the mean and the standard deviation of the Gaussian function, and f_0 is the central frequency. The signal and the corresponding frequency spectrum are shown in Figs. 4(a) and 4(b), respectively. Here, we choose $\mu = 2T_0$ and $\sigma = T_0/2$, and

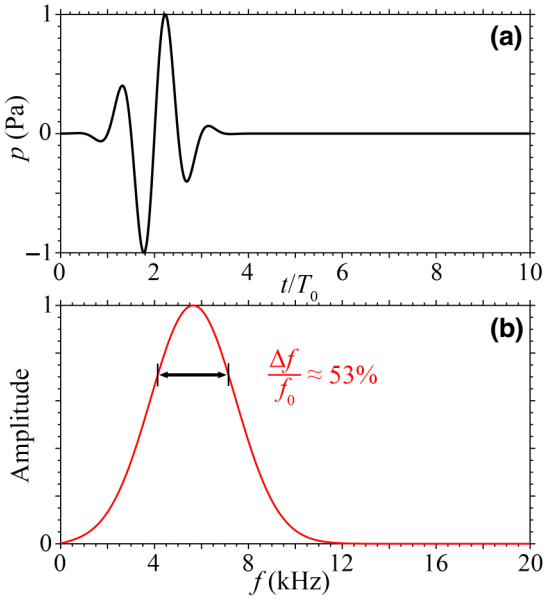

FIG. 4. (a) A broadband Gaussian wave packet with expectation $\mu = 2T_0$ and standard deviation $\sigma = T_0/2$. (b) Corresponding frequency spectrum for the sound signal in (a). The relative bandwidth for the signal is about 53%.

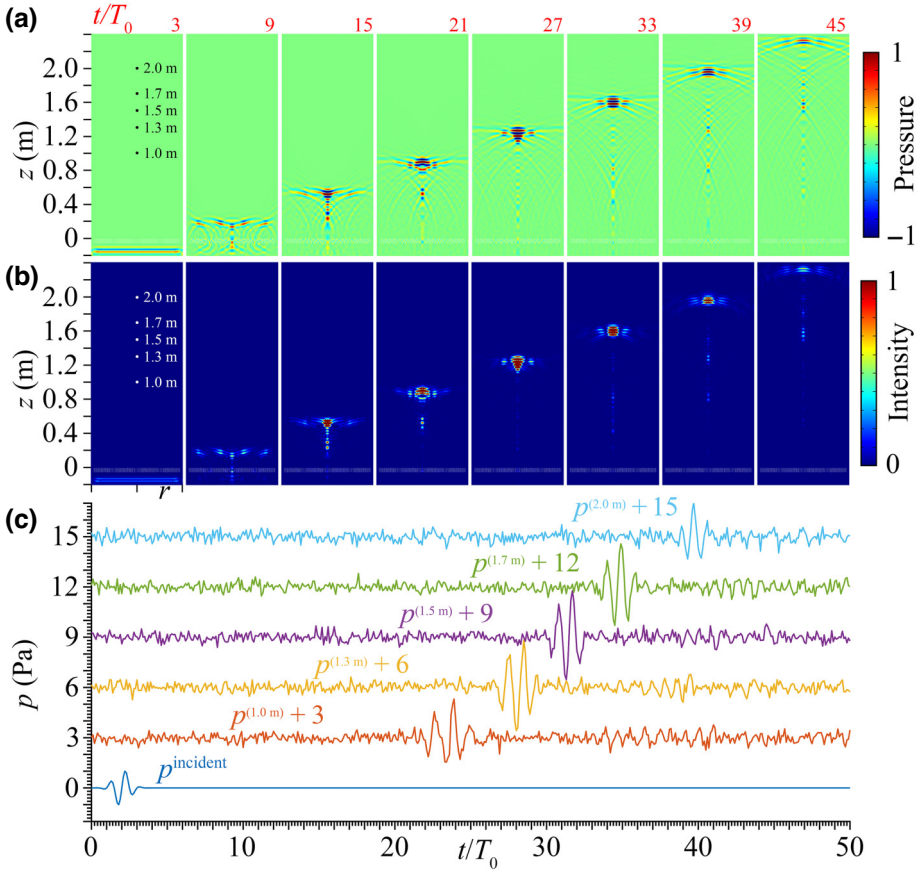

FIG. 5. Propagation of a pulse wave through the metalaser. (a) Simulated acoustic pressure fields and (b) intensity fields at different points in time. (c) Measured sound signals at several spatial locations as indicated by black dots in (a) [or white dots in (b)].

the relative bandwidth of the Gaussian pulse here is about 53%. The relative bandwidth is calculated by $\Delta f/f_0 = (f_2 - f_1)/f_0$, where f_1 and f_2 are the two cutoff frequencies at the -3-dB locations around the central frequency f_0.

We simulate the propagation of the pulse wave through the acoustic metalaser. Here, the simulations are conducted in the time domain ("transient domain") and the time resolution for the computation is $T_0/60$, with the spatial

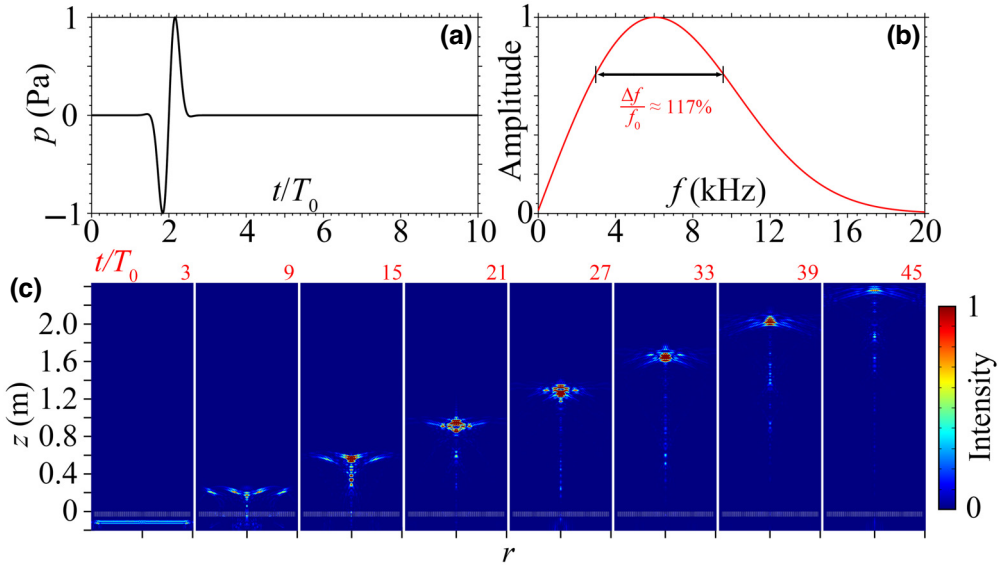

FIG. 6. Propagation of the pulse wave through the metalaser. (a) A broadband Gaussian wave packet with expectation $\mu = 2T_0$ and standard deviation $\sigma = T_0/5$. (b) Corresponding frequency spectrum for the sound signal in (a). (c) Acoustic intensity fields at different points in time.

resolution unchanged as described in the last section. Figures 5(a) and 5(b) show the simulated acoustic pressure fields and intensity fields at different points in time. It can be clearly observed that acoustic energy starts to converge after passing through the metalaser ($t \sim 6T_0$). The energy becomes more and more concentrated and the amplification is larger than 1 when $t > 12T_0$. Then the concentrated wave packet continues to propagate along the central z axis with the wave shape and the envelope kept almost unchanged [see Fig. 5(c) for the measured sound signals at several spatial locations as indicated by black dots in Fig. 5(a)].

To further examine the broadband performance of the acoustic metalaser for the convergence of acoustic energy, we simulate the propagation of a Gaussian wave packet with a broader bandwidth of about 117% [$\mu = 2T_0$ and $\sigma = T_0/5$ in Eq. (2)]. The signal and the spectrum for the wave packet are shown in Figs. 6(a) and 6(b), respectively. Figure 6(c) shows the acoustic intensity fields at different points in time. From the results, the metalaser can still focus the incident energy along the central z axis for a long propagation distance, which again proves the excellent ability of the metalaser proposed here for broadband acoustic energy convergence while the signal envelope is kept almost unchanged.

V. CONCLUSION

In summary, we propose an acoustic metalaser for the convergence of acoustic energy within a long propagation distance and a broad working frequency bandwidth. By carefully controlling the geometric parameters within the metalaser, we generate an acoustic Bessel beam with a central pressure maximum. Continuous sine waves of different frequencies and pulse waves with relative bandwidths of 53% and 117% are used to examine the performance of the metalaser via the finite-element method in both the frequency domain and the transient domain. Numerical and experimental results prove the ability and effectiveness of the metalaser proposed here for broadband energy concentration with the same structure without any changes. Our work should help further study of acoustic energy convergence and should find applications in many fields where manipulations of broadband acoustic waves are desired, such as acoustic imaging, ultrasound therapy, and particle manipulation, and in other broadband devices.

ACKNOWLEDGMENTS

The authors acknowledge the support of the National Natural Science Foundation of China (Grant No. 12204241), the Natural Science Foundation of Jiangsu Province (Grant No. BK20220924), the Fundamental Research Funds for the Central Universities (Grants No. 30923011019 and No. 020414380195), and the Undergraduate Research Program of Nanjing University of Science and Technology (Grant No. 202310288056).

[1] Jie Zhu, Johan Christensen, Jesper Jung, Luis Martin-Moreno, X. Yin, Lee Fok, Xiang Zhang, and F. J. Garcia-Vidal, A holey-structured metamaterial for acoustic deep-subwavelength imaging, Nat. Phys. **7**, 52 (2011).

[2] Xu-Dong Fan and Likun Zhang, Trapping force of acoustical Bessel beams on a sphere and stable tractor beams, Phys. Rev. Appl. **11**, 014055 (2019).

[3] Xu-Dong Fan and Likun Zhang, Phase shift approach for engineering desired radiation force: Acoustic pulling force example, J. Acoust. Soc. Am. **150**, 102 (2021).

[4] Guancong Ma and Ping Sheng, Acoustic metamaterials: From local resonances to broad horizons, Sci. Adv. **2**, e1501595 (2016).

[5] Steven A. Cummer, Johan Christensen, and Andrea Alù, Controlling sound with acoustic metamaterials, Nat. Rev. Mater. **1**, 1 (2016).

[6] Badreddine Assouar, Bin Liang, Ying Wu, Yong Li, Jian-Chun Cheng, and Yun Jing, Acoustic metasurfaces, Nat. Rev. Mater. **3**, 460 (2018).

[7] Xudong Fan, Xiaolong Huang, Yang Kang, Can Li, Ning Li, and Chunsheng Weng, Ultra-broadband bending beam and bottle beam based on acoustic metamaterials, Appl. Sci. **12**, 3025 (2022).

[8] Yong Li, Xue Jiang, Rui-qi Li, Bin Liang, Xin-ye Zou, Lei-lei Yin, and Jian-chun Cheng, Experimental realization of full control of reflected waves with subwavelength acoustic metasurfaces, Phys. Rev. Appl. **2**, 064002 (2014).

[9] Kun Tang, Chunyin Qiu, Manzhu Ke, Jiuyang Lu, Yangtao Ye, and Zhengyou Liu, Anomalous refraction of airborne sound through ultrathin metasurfaces, Sci. Rep. **4**, 1 (2014).

[10] Shubhi Bansal, Christabel Choi, James Hardwick, Biswajoy Bagchi, Manish K. Tiwari, and Sriram Subramanian, Transmissive labyrinthine acoustic metamaterial-based holography for extraordinary energy harvesting, Adv. Eng. Mater. **25**, 2201117 (2022).

[11] Yangbo Xie, Wenqi Wang, Huanyang Chen, Adam Konneker, Bogdan-Ioan Popa, and Steven A. Cummer, Wavefront modulation and subwavelength diffractive acoustics with an acoustic metasurface, Nat. Commun. **5**, 1 (2014).

[12] Xuefeng Zhu, Kun Li, Peng Zhang, Jie Zhu, Jintao Zhang, Chao Tian, and Shengchun Liu, Implementation of dispersion-free slow acoustic wave propagation and phase engineering with helical-structured metamaterials, Nat. Commun. **7**, 1 (2016).

[13] Yong Li, Xue Jiang, Bin Liang, Jian-chun Cheng, and Likun Zhang, Metascreen-based acoustic passive phased array, Phys. Rev. Appl. **4**, 024003 (2015).

[14] Yifan Zhu, Xudong Fan, Bin Liang, Jianchun Cheng, and Yun Jing, Ultrathin acoustic metasurface-based Schroeder diffuser, Phys. Rev. X **7**, 021034 (2017).

[15] Xudong Fan, Bin Liang, Jing Yang, and Jianchun Cheng, Illusion for airborne sound source by a closed layer with subwavelength thickness, Sci. Rep. **9**, 1750 (2019).

[16] Xu-Dong Fan and Likun Zhang, Acoustic orbital angular momentum Hall effect and realization using a metasurface, Phys. Rev. Res. **3**, 013251 (2021).

[17] Zhilin Hou, Xinsheng Fang, Yong Li, and Badreddine Assouar, Highly efficient acoustic metagrating with strongly coupled surface grooves, Phys. Rev. Appl. **12**, 034021 (2019).

[18] Yan Kei Chiang, Sebastian Oberst, Anton Melnikov, Li Quan, Steffen Marburg, Andrea Alù, and David A. Powell, Reconfigurable acoustic metagrating for high-efficiency anomalous reflection, Phys. Rev. Appl. **13**, 064067 (2020).

[19] Xu-Dong Fan, Yi-Fan Zhu, Bin Liang, Jing Yang, and Jian-Chun Cheng, Broadband convergence of acoustic energy with binary reflected phases on planar surface, Appl. Phys. Lett. **109**, 243501 (2016).

[20] He Gao, Zhongming Gu, Shanjun Liang, Shuowei An, Tuo Liu, and Jie Zhu, Coding metasurface for Talbot sound amplification, Phys. Rev. Appl. **14**, 054067 (2020).

[21] Yifan Zhu, Jie Hu, Xudong Fan, Jing Yang, Bin Liang, Xuefeng Zhu, and Jianchun Cheng, Fine manipulation of sound via lossy metamaterials with independent and arbitrary reflection amplitude and phase, Nat. Commun. **9**, 1 (2018).

[22] Yifan Zhu and Badreddine Assouar, Systematic design of multiplexed-acoustic-metasurface hologram with simultaneous amplitude and phase modulations, Phys. Rev. Mater. **3**, 045201 (2019).

[23] Rasha Al Jahdali and Ying Wu, High transmission acoustic focusing by impedance-matched acoustic meta-surfaces, Appl. Phys. Lett. **108**, 031902 (2016).

[24] Shuibao Qi, Yong Li, and Badreddine Assouar, Acoustic focusing and energy confinement based on multilateral metasurfaces, Phys. Rev. Appl. **7**, 054006 (2017).

[25] Jian Chen, Jing Xiao, Danylo Lisevych, Amir Shakouri, and Zheng Fan, Deep-subwavelength control of acoustic waves in an ultra-compact metasurface lens, Nat. Commun. **9**, 4920 (2018).

[26] Guangxin Liao, Zhenwei Wang, Congcong Luan, Jiapeng Liu, Xinhua Yao, and Jianzhong Fu, Broadband controllable acoustic focusing and asymmetric focusing by acoustic metamaterials, Smart Mater. Struct. **30**, 045021 (2021).

[27] Hao-Wen Dong, Chen Shen, Sheng-Dong Zhao, Weibao Qiu, Hairong Zheng, Chuanzeng Zhang, Steven A. Cummer, Yue-Sheng Wang, Daining Fang, and Li Cheng, Achromatic metasurfaces by dispersion customization for ultra-broadband acoustic beam engineering, Natl. Sci. Rev. **9**, nwac030 (2022).

[28] Xudong Fan, Yifan Zhu, Zihao Su, Ning Li, Xiaolong Huang, Yang Kang, Can Li, Chunsheng Weng, Hui Zhang, Bin Liang, *et al.*, Ultrabroadband and reconfigurable transmissive acoustic metascreen, Adv. Funct. Mater. **33**, 2300752 (2023).

[29] Yong Li, Bin Liang, Zhong-ming Gu, Xin-ye Zou, and Jian-chun Cheng, Reflected wavefront manipulation based on ultrathin planar acoustic metasurfaces, Sci. Rep. **3**, 1 (2013).